Nuclear Instruments and Methods in Physics Research A 1057 (2023) 168770

Contents lists available at ScienceDirect

Nuclear Inst. and Methods in Physics Research, A

journal homepage: www.elsevier.com/locate/nima

Full Length Article

Wakefield damping in a distributed coupling linear accelerator

Evan Ericson [a,b,*], Alexej Grudiev [a], Drew Bertwistle [b,c], Mark J. Boland [b,c]

[a] CERN, European Organization for Nuclear Research, 1 Espl. des Particules, Meyrin, 1221, Switzerland
[b] Department of Physics and Engineering Physics, University of Saskatchewan, 116 Science Place, Saskatoon, S7N 5E2, Canada
[c] Canadian Light Source, 44 Innovation Blvd, Saskatoon, S7N 2V3, Canada

ARTICLE INFO

Keywords:
Linear accelerator
Distributed coupling
Wakefield
Wake potential

ABSTRACT

The number of cells in a π-mode standing wave (SW) accelerating structure for the Compact Linear Collider (CLIC) project is limited by mode overlap with nearby modes. The distributed coupling scheme avoids mode overlap by treating each cell as independent. Designs of cells suitable for distributed coupling with strong wakefield suppression by waveguide damping have not previously been studied. In this paper we develop a SW cell to be used in a distributed coupling structure that can satisfy the CLIC transverse wake potential limit. From the middle cell of the CLIC-G* traveling wave (TW) structure, a SW cell is designed and then adapted to perform as a cell in a distributed coupling structure. Its wake potentials in an ideal case of open boundaries are reduced to satisfy the wake potential threshold. An electric boundary is added to the model to simulate total reflection at the distribution network. A horizontal coupler cell that connects to the distribution network such that the reflected wakefields remain similar to the open boundary case is simulated. A triplet module which takes advantage of cell-to-cell coupling to reduce reflected wake potential is presented.

1. Introduction

The main linear accelerator (LINAC) of the CLIC project uses accelerating structures to generate high-energy particles for particle physics experiments [1]. The current LINAC design uses TW X-band radio frequency (RF) accelerating structures shown in Fig. 1. These structures consist of 26 regular accelerating cells and two coupler cells, one upstream and the other downstream. The cell irises radii are tapered along the length of the structure from 3.15 mm to 2.35 mm to maintain a constant 100 MV/m gradient. All cells feature waveguides with silicon carbide loads to dissipate power from higher order modes (HOM) [2].

Recent work has shown converting the $2\pi/3$-mode TW structure (28 cells, 233 mm) to a π-mode SW structure (18 cells, 225 mm) increases the RF-to-beam efficiency by ~3% [3]. A SW structure operating in the π-mode is limited to the number of cells, N, given by Eq. (1).

$$\sqrt{\frac{Q_{0,\pi}\pi^2 k}{4}} > N. \tag{1}$$

where $Q_{0,\pi}$ is the quality factor, Q_0, of the π-mode and k is the coupling constant between adjacent cells. For a SW cell based on CLIC-G* cell shape, the maximum number of cells before mode overlap is 9. With this many cells, the π-mode is separated from the next adjacent mode by

$$\Delta f^{\pi}_{N,N-1} = f_r \frac{k\pi^2}{4N^2} = 2\,\text{MHz}. \tag{2}$$

Operating a side-coupled structure in the $\pi/2$-mode simultaneously increases the number of cells in a structure before mode overlap while keeping the shunt impedance high [4]. However, side-coupled geometries are not easily amenable to cells with four HOM waveguides. Distributed coupling topologies allow SW structures to increase the number of cells in a structure by treating each cell as independent. In this configuration, each accelerating cell is connected directly to the power source by a waveguide which runs parallel to the structure, rather than relying on cell-to-cell coupling [5,6]. Because the structure does not rely on coupling between cells, the cells' iris apertures can be made small to increase the shunt impedance. Distributed coupling schemes can also increase high-gradient performance by limiting the amount of power flow through the cell irises which are prone to RF breakdown events [7,8]. As the iris aperture decreases, the effects of wakefields increase [9]. Some existing designs reduce wakefields by using detuning such that problematic dipole modes add coherently ideally after the end of the bunch train [10]. Detuning can provide dipole modes with Q_{ext} = 1000 while CLIC requires modes with Q_{ext} ~ 10 or lower [11,12]. Other distributed coupling accelerator designs make use of slots to extract the wakefields that risk to perturb witness bunches [13,14]. In this work, we present the development of an RF accelerating cell suitable for a distributed coupling structure that satisfies the CLIC transverse wakefield requirement by using waveguide damping. Section 2 outlines the procedure followed to get a SW cell

* Corresponding author.
E-mail address: evan.ericson@psi.ch (E. Ericson).

https://doi.org/10.1016/j.nima.2023.168770
Received 9 June 2023; Received in revised form 3 October 2023; Accepted 7 October 2023
Available online 11 October 2023

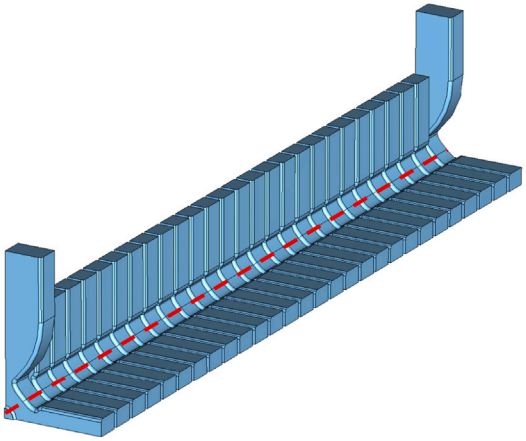

Fig. 1. Vacuum volume of the CLIC-G* TW structure for CLIC with quarter symmetry. The beam axis is shown as a red dashed line.

design. The cell is adapted first to include a power input and then further to reduce the wake potential of the cell. In Section 3 the reflected wake potential from a distribution network is analyzed and Section 4 describes cell designs capable of reducing the reflected wake potentials to an acceptable level. The final results are summarized in Section 5.

2. Open boundary wakes

The following procedure was used to develop a SW accelerating cell suitable for a distributed coupling structure for CLIC:

1. Choose a cell geometry with a direct connection to an external power source.
2. Evaluate the cell's accelerating mode frequency (f_0), quality factor (Q_0), shunt impedance (R), surface electric field (E_s/E_a), surface magnetic field (H_s/E_a) and Modified Poynting vector (S_c/E_a^2) [15] and verify they are similar to the values of the TW cells.
3. Determine if the cell is able to damp the transverse wake potentials below the threshold value of 6 V(pC m mm)$^{-1}$ [16] before a witness bunch arrives in the cell. The cell is simulated with an open boundary condition applied to the surface where the coupler meets a distribution network to represent a best-case scenario where the wakefields are extracted from the cell and dissipated completely outside the cell.
4. Determine if the cell is able to damp the transverse wake potentials below the threshold value before a witness bunch arrives in the cell when an electric, reflective, boundary condition is assigned to the coupler surface. This arrangement simulates a worst-case scenario where all wakefields extracted from the cell are reflected from the distribution network and return to the cell where they may act on following bunches.

If steps 2–4 were not satisfied after some parameter optimization, a new geometry was considered and the process restarted. An example of the boundary conditions for steps 3 and 4 are shown in Fig. 2. To reduce the simulation time and complexity, open boundary conditions were placed on the HOM waveguides simulating the wakefields extracted from the cell propagating outwards in the HOM waveguides without meeting any boundaries. In this way, the effect of the RF loads, in which the wakefield power is dissipated, located at the ends of the HOM waveguides, was effectively considered in the simulations. This approach eliminated the need of modeling the complex geometries of the RF loads in the simulations [2]. This method assumes all wakefield

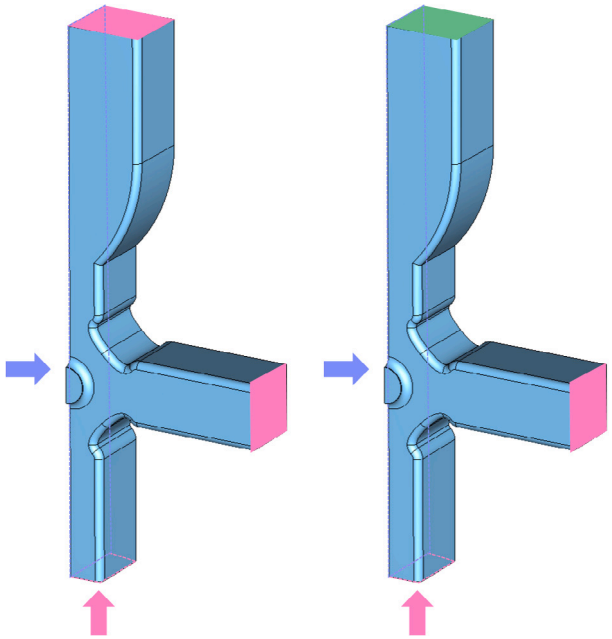

Fig. 2. Example boundary conditions for a cell considered in the development of a strongly damped accelerating cell for CLIC. In step 3, the HOM waveguides and the coupler waveguide were terminated with open boundaries (pink). When an electric boundary (green) was included in step 4, it was applied to the coupler waveguide while the HOM waveguides retained their open boundaries. The purple face was either electric or magnetic depending on the polarization of the wake potential being simulated.

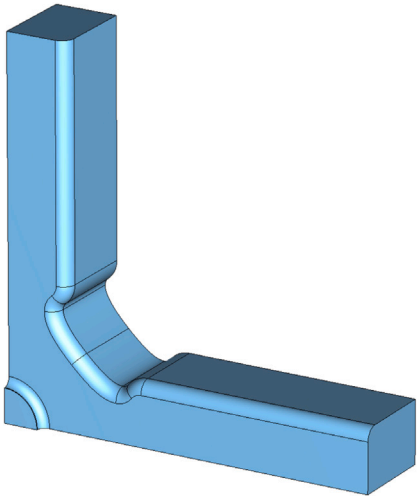

Fig. 3. Vacuum volume of an accelerating cell from the CLIC-G* TW structure for CLIC with quarter symmetry.

power is dissipated in the loads and there are no reflections from the loads back into the cell.

The middle cell of the tapered TW structure shown in Fig. 3 was chosen as a starting point for the design. The cell length was adjusted so the π-mode was synchronous with a relativistic beam. Parameters sweeps of the iris thickness and ellipticity were performed in CST's eigenmode solver [17] to select an iris shape that minimized the surface electric field. Sweeps of the outer wall parameters A0 and A2, described in [2] and shown in Fig. 4, confirmed the values of the TW cell also minimized the surface magnetic field for the SW cell. The outer wall radius, b, was adjusted to obtain the operating frequency. Once simulated, the cell had the RF parameters listed in Table 1. An accelerating structure having the same length as the TW structure based on this SW cell design would have an RF-to-beam efficiency of 31%.

Table 1
Geometry and RF parameters of SW cell.

Quantity	Unit	Value
Cell outer radius, b	mm	8.56
Iris aperture, a	mm	2.75
Iris thickness, d	mm	2.6
Iris ellipticity, e	mm	2.4
f_0	GHz	11.9945
Q_0	–	6927
R/Q_0	Ω/m	10,962
R	MΩ	75.93
E_s/E_a	–	1.80
H_s/E_a	mA/V	4.67
S_c/E_a^2	mA/V	0.35

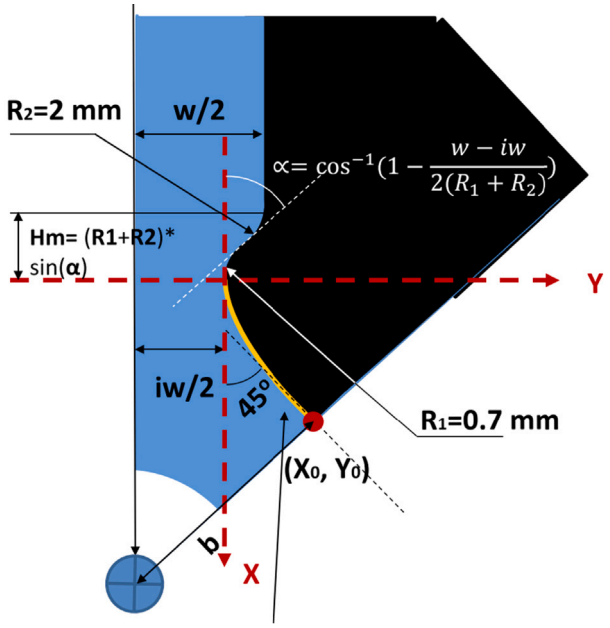

Fig. 4. Parameters of the CLIC normal cells [18]. The outer wall, shown in yellow, is described analytically by $Y = Y_0 + (X - X_0) + \left(\frac{X}{X_0} - 1\right)^2 \left(A_0 + A_1 \frac{X}{X_0} + A_2 \frac{X^2}{X_0}\right)$ where $Y_0 = \frac{b}{\sqrt{2}} - \frac{iw}{2}$, $X_0 = A_0 + Y_0$, $A_0 = 1.04\,\text{mm}$, $A_1 = A_0 - Y_0$ and A_2 is unitless.

A normal cell with four HOM waveguides is fed by cell-to-cell coupling. To make the cell applicable for a distributed coupling structure, a coupler cell was generated based on the TW coupling cell. The TW coupler cells have only two HOM waveguides and therefore we expected the wake potential of a structure with every unit cell having an identical design with the coupler cells would be higher than a structure with cells with four HOM waveguides. To reduce this effect, the SW coupler cell shown in Fig. 6 included only one coupler waveguide and three HOM waveguides.

The cell was matched to the source by adjusting the cell's outer radius and the aperture between the coupler waveguide and the cell. The x-polarization of the wake potential was found to be lower in amplitude than the y-polarization. The evaluated transverse wake potential of the coupler cell was above the threshold. A hybrid cell design with a HOM waveguide transition between the coupler waveguide and the cell, called a long slot cell, is shown in Fig. 5. Its transverse wake potential was between the wake potential of the coupler cell and four HOM waveguide cell at the second bunch position.

To decrease the wake potential below the threshold, two approaches were taken. First, the aperture of the HOM waveguides, iw, were increased. Changing the geometry in this way caused the Q_{ext} of the dominant dipole mode to decrease at the expense of a lower Q_0 and a larger expected temperature rise on the surface of the cell. For each

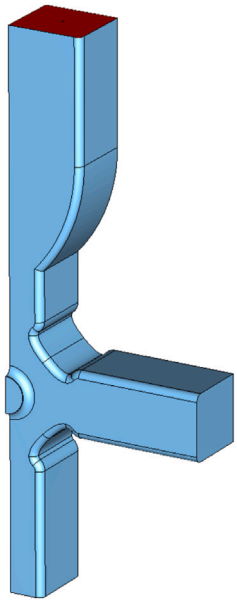

Fig. 5. Long slot cell geometry with half symmetry. The cell is matched by adjusting the cell outer radius and the length of the HOM waveguide connecting the cell to the wide coupler waveguide.

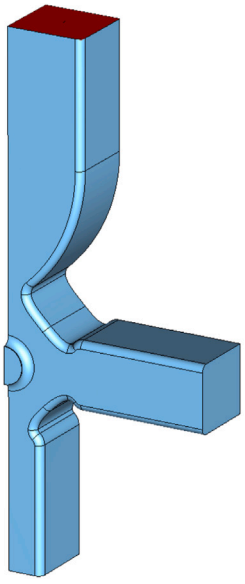

Fig. 6. Vacuum volume of a SW coupler cell based off the CLIC-G* TW coupler cell for CLIC with half symmetry.

iris aperture value simulated, the cells needed to be tuned to the correct frequency. The second approach was to increase the HOM waveguide widths, w. The wake potentials from these sweeps are shown in Fig. 7. The wake potential at the second bunch location was more sensitive to changes in w. A value of w = 10.7 mm was selected. Both polarization of the transverse wake potentials and their impedances are shown in Fig. 8.

3. Reflected wakes

To model the effect of a distribution network, parallel waveguide or otherwise, on the wake potential of the structure, an electric boundary

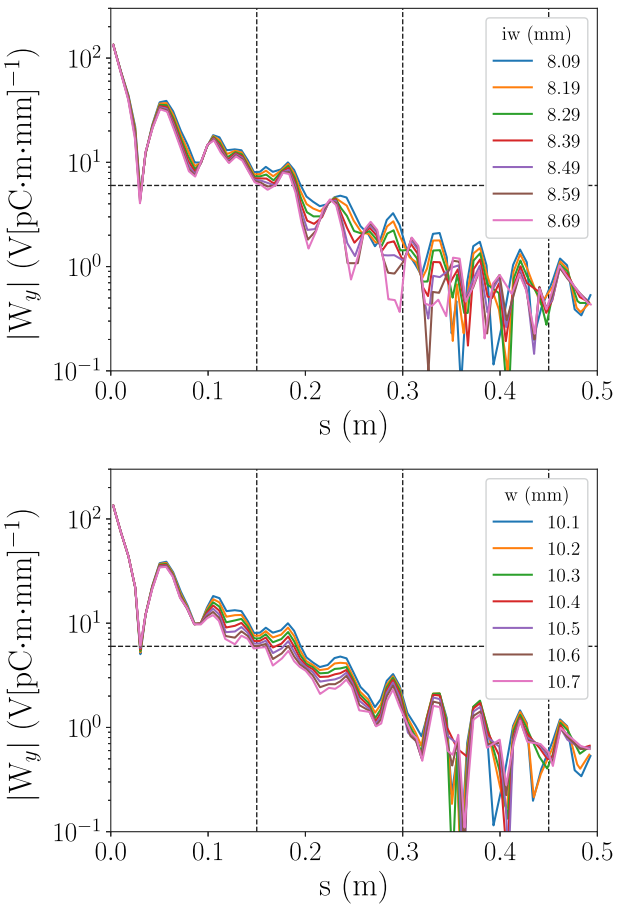

Fig. 7. Transverse wake potential envelopes of long slot cell with various HOM aperture widths, iw (top) and various HOM waveguide widths, w (bottom). The vertical dashed lines indicate witness bunch positions while the horizontal dashed line shows the wakepotential threshold.

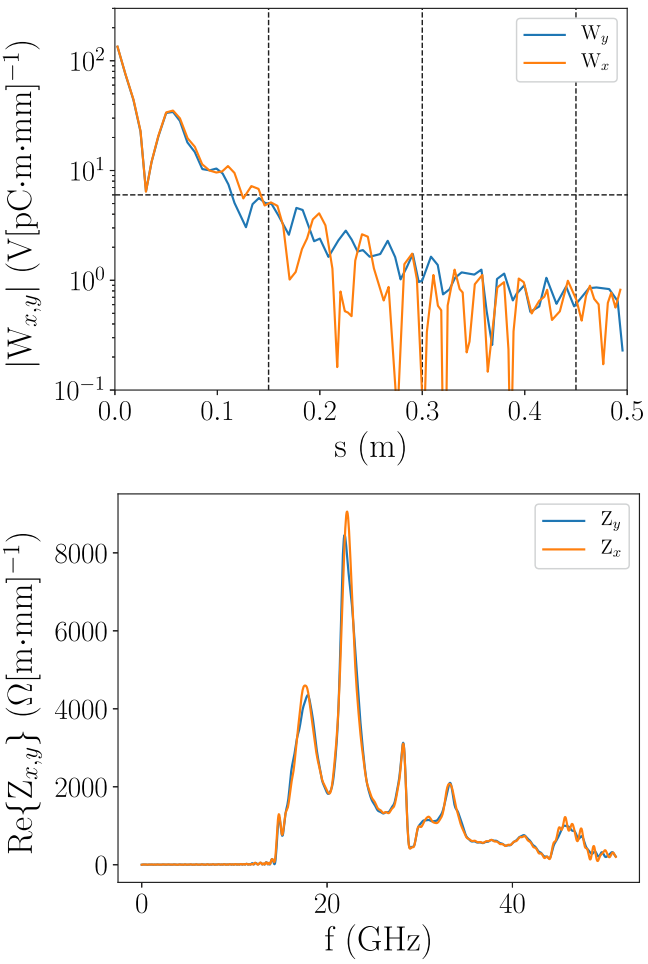

Fig. 8. Transverse wake potentials (top) and impedances (bottom) of long slot cell w = 10.7 mm (bottom).

was used to terminate, or short, the coupler waveguide as shown in Fig. 2. Fig. 9 shows the geometry simulated to include the effect of perfect reflection at the shorting plane set in the coupler waveguide.

An example of a reflected wake potential is shown in Fig. 10. After the drive bunch passes through the structure, the wakefields are extracted through the HOM waveguides. The fields propagating out of the cell through the coupler waveguide encounter the electric boundary and are reflected back into the cell. When the fields arrive back on-axis, the wake potential diverges from the open boundary case, exceeding the wake potential threshold. The position where the reflected wake potential diverges from the open boundary case is determined by the distance between the electric boundary and the beam axis which we call the "offset".

The position of the electric boundary represents the location of the distribution network relative to the beam. By adjusting the length of the offset the time elapsed between the excitation of the wakefields by the driving bunch and the arrival of the reflected wakefields back at the beam axis could be varied. Because the reflected wakefields were damped slowly, their magnitude witnessed by the next bunch exceeded the threshold. Increasing the HOM waveguide aperture, and width, which previously had an effect on the wake potential in the open boundary case, proved ineffective at reducing the reflected wake potential. The strategy of evaluating different iris geometries in an attempt to change the mode beating to form a minima at the bunches located during the reflected wake potential was unsuccessful.

The spectrogram of Fig. 11 shows the mode evolution of the reflected wake potential. Following excitation by a drive beam, the 17 and 22 GHz modes of Fig. 8 are quickly damped. The reflected wake potential first consists of modes near 17 GHz. While these modes are being damped, modes near 22 GHz arrive. The length of the reflected wake is (1) due to the difference in arrival time of the two sets of modes and (2) because of the slow damping of these modes. Increasing the offset changed the time at which the reflected wake potential differ from the open boundary wake potential and decreased the maximum amplitude of the reflected wake potential. A larger offset accentuated the difference in arrival time of the modes causing the cell to damp one set of modes at a time and the reflected wake potential duration increased as a result. The modes also spread in time due to dispersion in the waveguides. At an offset of 300 mm, the reflected wakepotential was still above the threshold at multiple bunch locations. We decided 300 mm coupler waveguides were not feasible in a realistic structure and abandoned extending the offset as a mechanism to damp the reflected wake potential.

4. Designs to reduce reflected wakefields

Two configurations were found to reduce the reflected wake potentials to an acceptable level. First, the horizontal coupler cell design shown in Fig. 12 feeds power to the cell from a coupler waveguide through an aperture in the side of one of the HOM waveguides. The aperture's dimensions and location allow power to enter the cell to establish the accelerating field while being sufficiently small that the

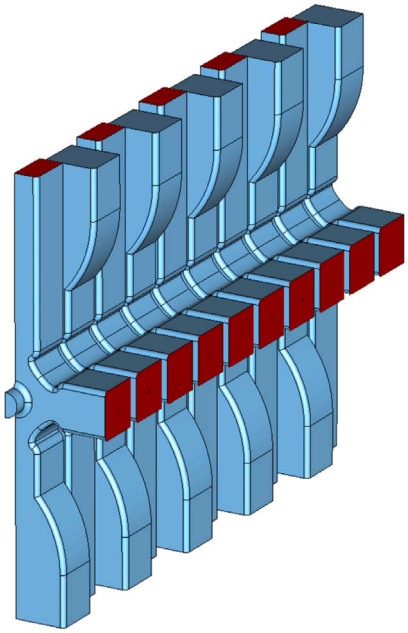

Fig. 9. Model simulated to obtain wake potential of reflected wakefields of the long slot cell using half symmetry. The coupler waveguides are slightly shorter than the HOM waveguides and experience an electric boundary. The model was parameterized to maintain these boundary conditions as the coupler waveguide length was increased.

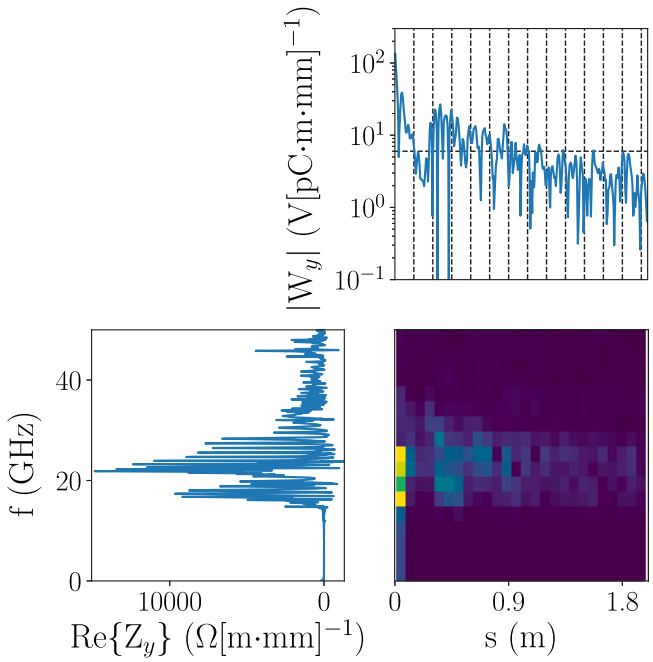

Fig. 11. Evolution of the mode content of the reflected wake potential with offset = 100 mm. The reflected transverse wake potential (top-right), the real transverse impedance (bottom left) and the spectrogram which shows the evolution of the impedance as a function of distance behind the drive beam.

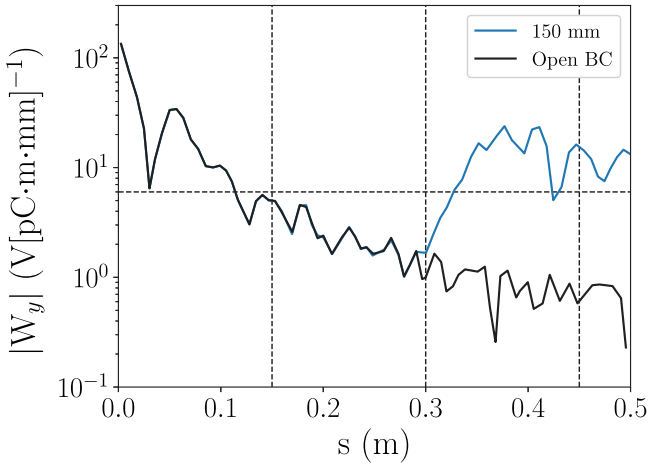

Fig. 10. Reflected transverse wake potential envelopes of long slot cell with w = 10.7 mm and offset = 150 mm.

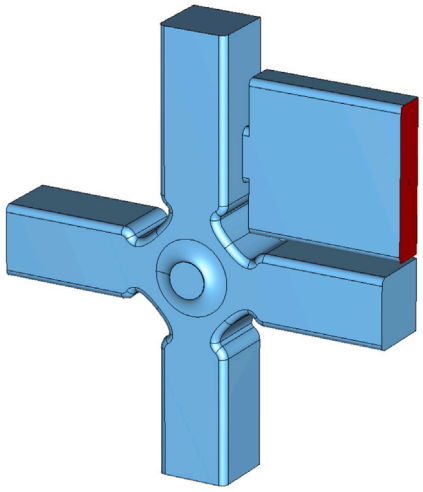

Fig. 12. Horizontal coupler cell geometry.

wakefields couple weakly to the coupler waveguide. The wakefields are damped in the HOM waveguides instead of being reflected at the coupler waveguide. The horizontal coupler cell has four HOM waveguides in contrast to the coupler cells of the TW structure which replace two HOM waveguides with coupler waveguides. Because the cutoff frequency of the HOM waveguides is above the operating frequency of 11.994 GHz, power of the fundamental mode does not propagate in the HOM waveguide and leakage of power from the fundamental mode to the HOM load can be minimized by placing the load an appropriate distance from the coupling aperture. The reflected wake potentials of Fig. 13 do not depend strongly on the offset meaning the horizontal coupler is transparent to the wakefields and a distribution network can be designed separately.

A second scheme where modules were formed of coupler cells and four HOM waveguide cells like the triplet shown in Fig. 14 also reduced the reflected wake potentials below the CLIC threshold. While distributed coupling structures consisting of only long slot cells had reflected wake potentials above the threshold at many bunch locations, an accelerating structure formed by periodic modules that consist of one long slot cell coupled with multiple unit cells that have four HOM waveguides reduces the reflected wake potential. The reflected wake potential amplitudes were lowered because of the reduced number of coupler waveguides from which reflections occur and the increased the number of HOM waveguides that damp the wakefields. The module takes advantage of the iris size of 2.75 mm, which is large enough to allow for coupling between cells. Operating a group of modules as a

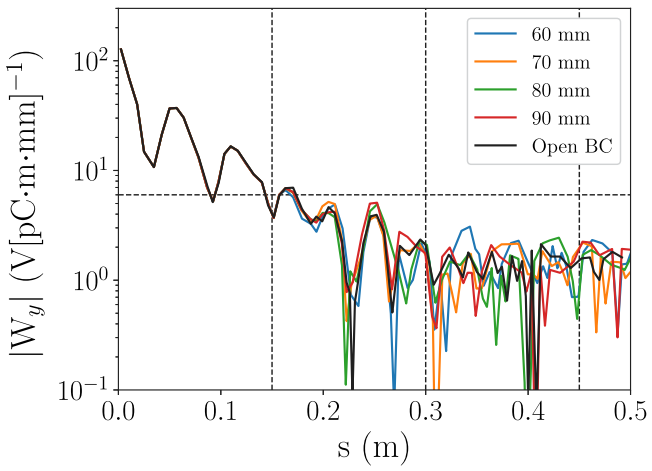

Fig. 13. Reflected transverse wake potential of horizontal coupler cell for various offsets. The cell design having wake potentials below the threshold for multiple offsets indicates the low reflected wake potential was not the result of fortuitous field cancellation that arises from a very specific offset.

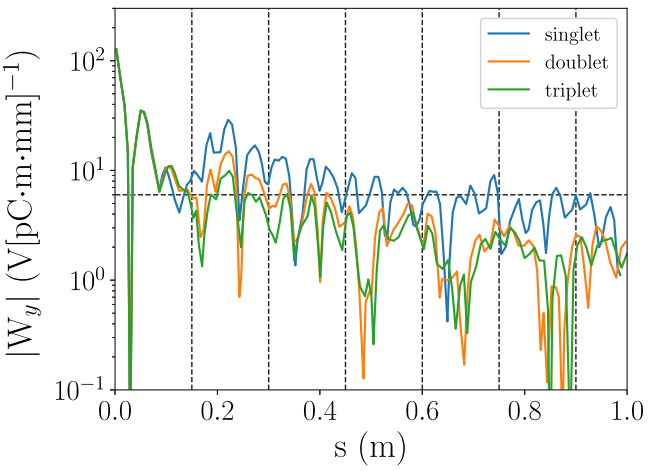

Fig. 15. Reflected transverse wake potentials of structures composed of singlets (long slot cell), doublet (one long slot and one four HOM waveguide cells) and triplet (one long slot and two four HOM waveguide cells).

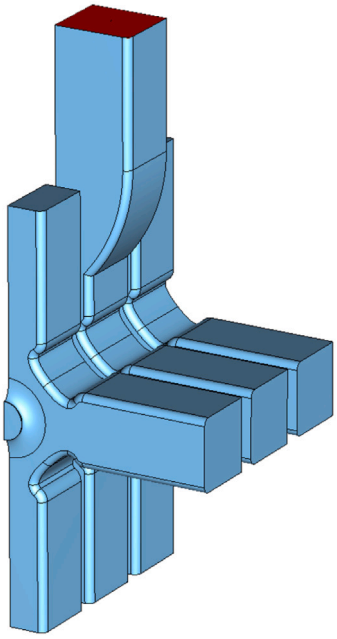

Fig. 14. Triplet module based on the long slot cell with half symmetry.

distributed coupling structure reduces the number of coupler waveguides required to feed the structure compared to distributed coupling structures where each cell has a feed to a power source. Fig. 15 shows the reflected wake potential amplitude decreases as the number of four HOM waveguide cells increases. The wake potential of the triplet is below the threshold at all bunch positions to 1 m. The outer radii of the cells in the doublet and triplets need to be tuned to achieve a flat longitudinal field. A triplet module where the coupler cell is a horizontal coupler cell combines a reduction of feed waveguides and effective mitigation of reflected wakefields.

We have demonstrated two different wakefield damping schemes for distributed coupling structures which meet the CLIC requirement. These simulations were performed using an electric boundary at the RF coupler waveguide termination, which represented the most demanding situation for the wakefield damping in the structure. We therefore expect these wakefield damping schemes to be viable in the realistic application scenario, where the RF coupler waveguide connects to the RF source, as opposed to being shorted.

5. Conclusion

A SW cell applicable to distributed coupling structures was developed. The HOM waveguide width was effective at lowering the open boundary wake potential at the second bunch position. The open boundary wake potentials were found to be less sensitive to changes in the HOM waveguide aperture than to changes of the HOM waveguide width. From the SW cell, two configurations were developed to give transverse reflected wake potentials below the CLIC threshold. The wakefields of the horizontal coupler cell couple weakly to the high power waveguide and are kept close to open boundary levels. The triplet module increases the number of HOM waveguides and decreases the number of coupler waveguides from which reflections originate to keep the reflected wake potential low. The presented cell designs can provide 100 MV/m gradient while loaded with the CLIC beam. Distributed coupling structures formed of these cells can provide an RF-to-beam efficiency of 31%.

Declaration of competing interest

The authors declare that they have no known competing financial interests or personal relationships that could have appeared to influence the work reported in this paper.

Data availability

Data will be made available on request.

Acknowledgments

This work was supported by CERN, Switzerland and the University of Saskatchewan, Canada. We would like to thank Ping Wang and Walter Wuensch for their interest in and discussions about this work.

References

[1] M. Aicheler, P. Burrows, M. Draper, T. Garvey, A Multi-TeV Linear Collider Based on CLIC Technology, Tech. rep., 2012, http://dx.doi.org/10.5170/CERN-2012-007, URL https://cds.cern.ch/record/1500095?ln=en.

[2] H. Zha, A. Grudiev, Design and optimization of Compact Linear Collider main linac accelerating structure, Phys. Rev. Accel. Beams 19 (11) (2016) 111003, http://dx.doi.org/10.1103/PhysRevAccelBeams.19.111003, URL https://link.aps.org/doi/10.1103/PhysRevAccelBeams.19.111003.

[3] V. Khan, A standing wave structure possibility for CLIC main LINACs, in: International Workshop on Breakdown Science and High Gradient Technology HG2013, Trieste, Italy, 2013, URL https://indico.cern.ch/event/231116/contributions/1542988/attachments/383424/533356/HGWS_03.06.13_VFK.pdf.

[4] T. Wangler, RF Linear Accelerators, first ed., 1998.

[5] S. Tantawi, M. Nasr, Z. Li, C. Limborg, P. Borchard, Design and demonstration of a distributed-coupling linear accelerator structure, Phys. Rev. Accel. Beams 23 (9) (2020) 092001, http://dx.doi.org/10.1103/PhysRevAccelBeams.23.092001.

[6] Y. Jiang, J. Shi, H. Zha, J. Liu, X. Lin, H. Chen, Analysis and design of parallel-coupled high-gradient structure for ultrashort input power pulses, Phys. Rev. Accel. Beams 24 (11) (2021) 112002, http://dx.doi.org/10.1103/PhysRevAccelBeams.24.112002.

[7] V.A. Dolgashev, S.G. Tantawi, Study of basic RF breakdown phenomena in high gradient vacuum structures, in: Proceedings of Linear Accelerator Conference LINAC2010, Tsukuba, Japan, 2010, pp. 1043–1047, URL https://accelconf.web.cern.ch/LINAC2010/papers/fr105.pdf.

[8] E.I. Simakov, V.A. Dolgashev, S.G. Tantawi, Advances in high gradient normal conducting accelerator structures, Nucl. Instrum. Methods Phys. Res. A 907 (February) (2018) 221–230, http://dx.doi.org/10.1016/j.nima.2018.02.085.

[9] K.L.F. Bane, Short range dipole wakefields in accelerating structures for the NLC 94309 (March) (2003) 1–13, URL https://www-project.slac.stanford.edu/lc/ilc/TechNotes/LCCNotes/PDF/LCC-0116.pdf.

[10] R.A. Rimmer, Extraction and absorption of higher order modes in room temperature accelerators, in: Worskhop on Microwave-Absorbing Materials for Accelerators, Newport News, VA, February 22-24, 1993, 1993, URL https://escholarship.org/uc/item/5vk3f1mk#author.

[11] K.L. Bane, T.L. Barklow, M. Breidenbach, C.P. Burkhart, E.A. Fauve, A.R. Gold, V. Heloin, Z. Li, E.A. Nanni, M. Nasr, M. Oriunno, J.M. Paterson, M.E. Peskin, T.O. Raubenheimer, S.G. Tantawi, An Advanced NCRF Linac Concept for a High Energy e^+e^- Linear Collider, Tech. rep., 2018, arXiv:1807.10195, URL http://arxiv.org/abs/1807.10195.

[12] A. Grudiev, W. Wuensch, Design of the CLIC main linac accelerating structure for CLIC conceptual design report, in: Proceedings of Linear Accelerator Conference LINAC2010, 2010, URL https://cds.cern.ch/record/1346987?ln=en.

[13] D. Kim, S. Biedron, Z. Li, E. Simakov, Design study of HOM couplers for the C-Band accelerating structure, IPAC2022 (2022) 1561–1563, http://dx.doi.org/10.18429/JACoW-IPAC2022-TUPOMS057.

[14] D. Kim, E.I. Simakov, Z. Li, Study of HOM couplers for the C-band accelerating structure, 2023.

[15] A. Grudiev, W. Wuensch, A new local field quantity describing the high gradient limit of accelerating structures, Phys. Rev. Special Top. - Accel. Beams 12 (2009) 1–9, http://dx.doi.org/10.1103/physrevstab.12.102001.

[16] D. Schulte, Multi-bunch calculations in the CLIC main linac, in: Proceedings, 23rd Conference, PAC'09, Vancouver, Canada, May 4-8, 2009, 2010, URL http://accelconf.web.cern.ch/AccelConf/PAC2009/papers/fr5rfp055.pdf.

[17] Computer simulation technology, CST studio suite, URL www.3ds.com/products-services/simulia/products/cst-studio-suite/.

[18] H. Zha, A. Grudiev, J. Liu, RF design and parameters of 2015 re-baselined 3TeV CLIC main linac AS at 12 GHz with compact couplers: CLIC-G* or TD261.8_R1_CC, 2015.